Computational Coupled Method for Multiscale and Phase Analysis

Moonho Tak
Research Professor
e-mail: pivotman@hanyang.ac.kr

Duhee Park
Associate Professor
e-mail: dpark@hanyang.ac.kr

Taehyo Park[1]
Professor
e-mail: cepark@hanyang.ac.kr

Department of Civil and Environmental Engineering,
Hanyang University,
Seoul 133-791, Korea

On micro scale the constitutions of porous media are effected by other constitutions, so their behaviors are very complex and it is hard to derive theoretical formulations as well as to simulate on macro scale. For decades, in order to escape this complication, the phenomenological approaches in a field of multiscale methods have been extensively researched by many material scientists and engineers. Their theoretical approaches are based on the hierarchical multiscale methods using a priori knowledge on a smaller scale; however it has a drawback that an information loss can be occurred. Recently, according to a development of the core technologies of computer, the ways of multiscale are extended to a direct multiscale approach called the concurrent multiscale method. This approach is not necessary to deal with complex mathematical formulations, but it is noted as an important factor: development of computational coupling algorithms between constitutions in a porous medium. In this work, we attempt to develop coupling algorithms in different numerical methods finite element method (FEM), smoothed particle hydrodynamics (SPH) and discrete element method (DEM). Using this coupling algorithm, fluid flow, movement of solid particle, and contact forces between solid domains are computed via proposed discrete element which is based on SPH, FEM, and DEM. In addition, a mixed FEM on continuum level and discrete element model with SPH particles on discontinuum level is introduced, and proposed coupling algorithm is verified through numerical simulation. [DOI: 10.1115/1.4023776]

Keywords: coupled method, porous media, finite element method, discrete element method, smoothed particle hydrodynamics, multiscale model

1 Introduction

The computational multiscale method is one of the powerful approaches in modern materials science and engineering because it can simulate accurate behaviors of real materials. This multiscale is conceptually categorized into hierarchical and concurrent method according to its approach about length scale. The hierarchical method, which is called information-passing method, is used to develop constitutive models on a larger scale, and this is expressed in terms of variables of smaller scale. The effective properties from the smallest scale are defined on representative volume element (RVE), and it is substituted into properties of a larger scale as constitutive equations. This procedure has advantages that heterogeneous properties in a smaller domain can be homogenized, moreover as using that computational cost is relatively cheaper than another multiscale method. In order to solve behavior of porous media, a hierarchical multiscale method is one of the interesting topics because porous media have particulars: highly heterogeneous and interactional nonlinearity between solid, fluids and gases on smaller scale. For incompressible fluid flow in porous media, Hou and Wu [1] developed a multiscale method for solving second-order elliptic problems characterized by highly heterogeneous and oscillation coefficients. This method provides a convenience to apply computational parallel algorithms by fully decomposed elements. Schrefler et al. [2] researched a multiscale method for the unsaturated porous media for hydration. In their study, they dealt with the mixed FEM comprised of fluid pressure, gas pressure, temperature, and displacements. Also, Arrhenius-type constitutive equation, which is derived by thermodynamic approach, is used to simulate long term hydration and chemical reaction of concrete at early age. In addition, Kippe et al. [3] reviewed with three different multiscale methods for elliptic problems of porous media: multiscale mixed FEM upscaling method, and the multiscale finite volume method. Later, Hajibeygi and Jenny [4] attempted to develop a multiscale finite volume method for compressible multiphase flow in porous media (parabolic problems). Most recently, Zhang et al. [5], respectively, developed the multiscale finite element method (MSFEM) and the upscaling FEM in order to analyze consolidation of coupled solid with fluid motion. The main idea of MSFEM is to construct base functions obtained from smaller scale information. The base functions for behavior of solid and fluid flow are applied into mixed finite element formulation on macroscopic. However, these hierarchical methods have a shortcoming that information lose can be occurred when homogenized and assumed effective material properties are determined in RVE domains.

On the other hand, the concurrent methods do not rely on any assumptions such as RVE, boundary conditions, and do not require a priori knowledge from physical quantities at smaller scale. They are directly connected to different scale methods like molecular dynamics (MD)-FEM, or DEM-FEM. Therefore, in this method, it is main key to define connectivity between different descriptions. However, although this method provides better accurate results than hierarchical method, it has been less researched because computational cost is expensive. Fortunately, the exponential growth of computer hardware excessively spurs the development of concurrent methods in engineering and science now. The researches about concurrent methods for porous media have been concentrated in the soil scope by using coupling algorithms between solid and fluid phase. El Shamy and Zeghal [6] and Zeghal and El Shamy [7] proposed the DEM method using the drag forces for liquefaction of saturated porous media.

[1]Corresponding author.

Manuscript received June 4, 2012; final manuscript received October 9, 2012; published online March 28, 2013. Assoc. Editor: Xi Chen.

In their research, DEM in micro scale and Navier–Stokes model of fluid flow in meso scale are coupled with the drag forces. Further, Elmekati and El Shamy [8] extended this method with multi time increments between DEM and FEM. Shafipour and Soroush [9] were also proposed fluid coupled DEM method, but they assumed that fluid flow in porous media is dominated by Darcy's law in macroscopic cells. To couple between DEM and cells fluid forces on particles are taken account in frame of Ergun's semi empirical relations. On the other hand, Muguruma et al. [10], Soulie et al. [11], Abu Bakar et al. [12], El Shamy and Groger [13], and Scholtes et al. [14] introduced fluid coupled DEM for unsaturated porous media. They considered noncontact forces from liquid bridges as capillary between spherical particles. This research is one of the interesting topics for unsaturated porous, because constitutive equations for unsaturated porous media in continuum level are sophisticated. However, their approach is limited to use ideal spherical particles despite almost natural materials have sharp corners. Consequently, ideal spherical particles in DEM arise from uncertain behavior for porous media. In addition, coupled SPH with DEM have been also introduced by Tartakovsky and Meakin [15], Tartakovsky and Meakin [16], and Tartakovsky et al. [17]. In their research, coupled interactions are expressed to no-slip boundary condition, pairwise particle forces. Especially, Li et al. [18] developed new characteristic based SPH method in which fluid flow in pore relative to the deformed solid particles. Further, direct numerical simulation-SPH method by Berry et al. [19] has been proposed in frame of porous materials.

The main issue of concurrent multiscale method for porous media is how to combine different numerical approaches with coupling mechanism. On discontinuum level, DEM is the most representative numerical method for simulation of solid motion, and SPH is suited for fluid flow in pore. On continuum level, FEM is the best solution in order to obtain fluid pressure and displacements. On the other hand, DEM or SPH has an advantage that accurate results can be obtained, but it has a drawback that it is hard to find approaching particles called particle detection, and numerical efficiency can be caused by this problem. Furthermore, if DEM particles have corners, instability can be occurred at contact of corner to corner.

To remedy these drawbacks, the coupling algorithm between these numerical methods is proposed. Especially, DEM particle embedded SPH particle is introduced and verified its excellence for detection of near DEM particles and definition of contact forces between DEM particles. For this, first finite element formulation for saturated porous media, DEM, and SPH methods are reviewed, then a coupling algorithm is introduced. Finally, the proposed method is verified with numerical examples.

2 Mixed Finite Element Formulation for Saturated Porous Media

2.1 Governing Equations for Saturated Porous Media. The governing equations for saturated porous media can be derived from the mass balance equation, momentum balance equation and constitutive equations. This derivation is based on Biot's theory [20] represented by microscopic relationship between constituted materials.

The momentum balance equations can be defined as follows:

$$\nabla \cdot \boldsymbol{\sigma} + \rho \boldsymbol{b} = \mathbf{0} \tag{1}$$

where $\boldsymbol{\sigma}$ is the total stress tensor, ρ is the density on total phase, and $\boldsymbol{b}$ is the body force vector.

In Eq. (1), the total stress tensor $\boldsymbol{\sigma}$ can be divided into effective stress tensor $\boldsymbol{\sigma}''$ represented average stress for pure solid skeleton in saturated porous media and the fluid pressure p^f [21]

$$\nabla \cdot (\boldsymbol{\sigma}'' - \mathbf{I}p^f) + \rho \boldsymbol{b} = 0 \tag{2}$$

where $\mathbf{I}$ is the identity tensor.

In addition to the momentum balance equations, the mass balance equation of saturated porous media can be derived as starting from equation of continuity on each phase. The equations of continuity on solid phase and fluid phase can be defined as follows, respectively:

$$\frac{D^s(1-n)\rho^s}{Dt} + (1-n)\rho^s \nabla \cdot \boldsymbol{v}^s = 0 \tag{3}$$

$$\frac{D^s n\rho^f}{Dt} + \nabla \cdot \left(n\rho^f \boldsymbol{v}^{fs}\right) + n\rho^f \nabla \cdot \boldsymbol{v}^s = 0 \tag{4}$$

where (D^s/Dt) is the operation of material time derivative on solid phase, n is the porosity, ρ^s is the density of solid, $\boldsymbol{v}^s$ is velocity vector of solid particle, ρ^f is the density of fluid, $\boldsymbol{v}^{fs}$ is the relative velocity vector represented $\boldsymbol{v}^{fs} = \boldsymbol{v}^f - \boldsymbol{v}^s$. This velocity can be substituted by Darcy's law

$$\boldsymbol{v}^{fs} = \frac{\mathbf{k}}{\mu^f}\left(-\nabla p^f + \rho^f \boldsymbol{g}\right) \tag{5}$$

where $\boldsymbol{k}$ is the permeability tensor, μ^f is the dynamic viscosity for fluid, and $\boldsymbol{g}$ is the gravity vector.

In addition to Darcy's law, in Eqs. (3) and (4), the material time derivatives of densities on solid and fluid phase can be represented by constitutive equations introduced by Lewis and Schrefler [22], respectively

$$\frac{D^s\rho^s}{Dt} = \frac{\rho^s}{1-n}\left[(\alpha - n)\frac{1}{K^s}\frac{D^s p^s}{Dt} - \beta^s(\alpha - n)\frac{D^s T}{Dt} - (1-\alpha)\nabla \cdot \boldsymbol{v}^s\right] \tag{6}$$

$$\frac{1}{\rho^f}\frac{D^s\rho^f}{Dt} = \frac{1}{K^f}\frac{D^s p^f}{Dt} \tag{7}$$

in which, α is Biot's constant, p^s is the pressure on solid phase, K^s and K^f are the bulk modulus of solid phase and fluid phase, respectively, β^s is the thermal expansion coefficient, and T is the temperature.

Moreover, the pressure on solid phase p^s can be converted into the pressure on fluid phase p^f with fluid saturation S^f for porous media as follows:

$$p^s = p^f S^f \tag{8}$$

When a porous medium is isothermal, saturated and small deformation, the thermal expansion coefficient $\beta^s = 0$ in Eq. (6), fluid saturation $S^f = 1$ in Eq. (8), and $(D^s/Dt) = (\partial/\partial t)$. Substituting Eqs. (4)–(8) into Eq. (3), we can, finally, obtain the mass balance equation for saturated porous media as follows:

$$\left(\frac{\alpha - n}{K^s} + \frac{n}{K^f}\right)\frac{\partial p^f}{\partial t} + \alpha \nabla \cdot \boldsymbol{v}^s + \frac{1}{\rho^f}\nabla \cdot \left(\frac{\boldsymbol{k}}{\mu^f}\left(-\nabla p^f + \rho^f \boldsymbol{g}\right)\right) = 0 \tag{9}$$

2.2 Mixed Finite Element Formulation. For finite element procedure, Eqs. (2) and (9) can be represented into mixed finite element formulation using shape functions. First in order to derive weak form the Dirichlet boundary conditions on displacements boundary Γ^s and on fluid pressures boundary Γ^f, and Neumann boundary conditions on traction boundary Γ^t and on flux boundary Γ^q are applied into these equation in the total domain Ω. Second, test functions, which are composed with shape function for solid phase N^s, shape function for fluid phase N^f, approximated displacements vector $\bar{\boldsymbol{u}}^s$ and approximated fluid pressure vector $\bar{\boldsymbol{p}}^f$, can be substituted into weak form. Finally, we can obtain mixed finite element formulation as follows:

$$\mathbf{K}\bar{\boldsymbol{u}}^s - \mathbf{C}\bar{\boldsymbol{p}}^f = \boldsymbol{f}^s \tag{10}$$

$$\mathbf{C}^{\mathrm{T}}\frac{\partial \bar{\boldsymbol{u}}^s}{\partial t}+\mathbf{S}\frac{\partial \bar{\boldsymbol{p}}^f}{\partial t}+\mathbf{D}\bar{\boldsymbol{p}}^f=\boldsymbol{f}^f \tag{11}$$

where,

$$\mathbf{K}=\int_\Omega\left[(\nabla N^s)^{\mathrm{T}}\mathbf{C}_{\mathrm{T}}\nabla N^s\right]\mathrm{d}\Omega$$

is the stiffness matrix, where the $\mathbf{C}_{\mathrm{T}}$ is the constitutive matrix, $\mathbf{C}=\int_\Omega\left[(\nabla N^s)^{\mathrm{T}}\mathbf{I}N^f\right]\mathrm{d}\Omega$ is the coupled matrix,

$$\boldsymbol{f}^s=\int_\Omega N^s\rho\boldsymbol{b}\mathrm{d}\Omega-\int_{\Gamma^t}N^s\bar{\boldsymbol{t}}\mathrm{d}\Gamma$$

is the external force for the solid phase, where $\bar{\boldsymbol{t}}$ is traction vector

$$\mathbf{S}=\int_\Omega\left[(N^f)^{\mathrm{T}}\left(\frac{\alpha-n}{K^s}+\frac{n}{K^f}\right)N^f\right]\mathrm{d}\Omega$$

is the compressible matrix,

$$\mathbf{D}=\int_\Omega\left[(\nabla N^f)^{\mathrm{T}}\frac{\mathbf{k}}{\mu^f}\nabla N^f\right]\mathrm{d}\Omega$$

is the drainable matrix,

$$\boldsymbol{f}^f=\int_\Omega\left[(\nabla N^f)^{\mathrm{T}}\frac{\mathbf{k}}{\mu^f}\rho^f\boldsymbol{g}\right]\mathrm{d}\Omega-\int_{\Gamma^q}\left[N^f\frac{\bar{q}}{\rho^f}\right]\mathrm{d}\Gamma$$

is the external force for the fluid phase.

3 DEM.

Discrete element method is a numerical method for analysis of granular materials. Although the real material on discontinuum level is too complex, it can be simulated by simplified spherical particles, and the motions of spherical particles are governed by Newton's second law in which each particle is moved by forces. The handle of this method is simpler than FEM, but two issues, particle detection and contact force, should be resolved reasonably.

3.1 Governing Equations.

The governing equation for particle motion is comprised of translation and rotation. The translational motion of rigid spherical particle i can be defined as follows:

$$m_i\ddot{\boldsymbol{u}}_i=\boldsymbol{F}_i \tag{12}$$

where m_i is mass, $\ddot{\boldsymbol{u}}_i$ is acceleration vector, and $\boldsymbol{F}_i$ is total force vector for particle i, respectively. In addition, rotational motion is expressed such that

$$J_i\dot{\boldsymbol{\omega}}_i=\boldsymbol{T}_i \tag{13}$$

in which J_i is the moment of inertia, $\dot{\boldsymbol{\omega}}_i$ is the angular velocity vector, and $\boldsymbol{T}_i$ is the moment vector for particle i, respectively.

The total force vector $\boldsymbol{F}_i$ in Eq. (12) can be divided a variety forces as external force vector $\boldsymbol{F}_i^e$, contact force vector $\boldsymbol{F}_{ij}^c$, fluid pressure vector $\boldsymbol{F}_i^f$, and gravity force vector $\boldsymbol{F}_i^g$.

$$\boldsymbol{F}_i=\boldsymbol{F}_i^e+\sum_j\boldsymbol{F}_{ij}^c+\boldsymbol{F}_i^f+\boldsymbol{F}_i^g \tag{14}$$

where j is expressed opposite particles in computational domain.

3.2 Contact Force $\boldsymbol{F}_{ij}^c$.

In Eq. (14), contact force $\boldsymbol{F}_{ij}^c$ can be decomposed into two forces according to direction; normal force and friction force. The most common model for this is spring-dashpot model proposed by Cundall and Stack [23]. Considering cohesive effect, the contact normal force $\boldsymbol{F}_n^c$ and the contact tangential force $\boldsymbol{F}_t^c$ can be defined as follows, respectively

$$\boldsymbol{F}_n^c=K_n\boldsymbol{u}_n+C_n\dot{\boldsymbol{u}}_n \tag{15}$$

$$\left\|\boldsymbol{F}_t^c\right\|=K_t\|\boldsymbol{u}_t\|+C_t\|\dot{\boldsymbol{u}}_t\| \tag{16}$$

where K_n is interface stiffness in the normal direction, $\boldsymbol{u}_n$ is displacement, C_n is a viscous damping coefficient and $\dot{\boldsymbol{u}}_n$ is relative velocity in the normal direction, K_t is interface stiffness in the tangential direction, $\boldsymbol{u}_t$ is relative displacement, C_t is a viscous damping coefficient, and $\dot{\boldsymbol{u}}_t$ is relative velocity in tangential direction. It is note that these relationships are instantaneously broken when forces are over a capacity of strength [24].

Assuming that damping force does not considered, we can consider a slip by normal force after cohesive effect is broken between two particles ($\left\|\boldsymbol{F}_t^c\right\|>R_t$, R_t is the limited strength for tangential direction). Contact tangential force should be redefined with Coulomb friction theory

$$\left\|\boldsymbol{F}_t^c\right\|=\mu\left\|\boldsymbol{F}_n^c\right\| \tag{17}$$

where μ is the friction coefficient. However, this method has a limitation that it is difficult to determined stiffness and damping properties between two particles; therefore this method is rigorous to use although numerical procedure is straightforward.

In addition to spring-dashpot model, Hertz [25] proposed elastic contact force in the normal direction between spherical particles. Since his model exhibits a nonlinear relationship, it is appropriate to simulate large movements of particle

$$\boldsymbol{F}_n^c=\frac{4}{3}\left(\frac{1-\nu_a^2}{E_a}+\frac{1-\nu_b^2}{E_b}\right)^{-1}\sqrt{R}\delta^{3/2} \tag{18}$$

where E is elastic modulus, ν is Poisson ratio for each particles a and b, $R=R_AR_B/(R_A+R_B)$ is the equivalent radius, and δ is the maximum overlapping distance.

4 SPH

SPH is one of the meshfree methods for obtaining approximate solutions of fluid dynamics. In this method, characteristics particles based on Lagrangian description are defined by properties of near particles in smoothing length as Fig 1.

4.1 Governing Equations.

The formulations for SPH are based on kernel approximation or kernel functions. This kernel approximation can be represented with smoothing kernel function

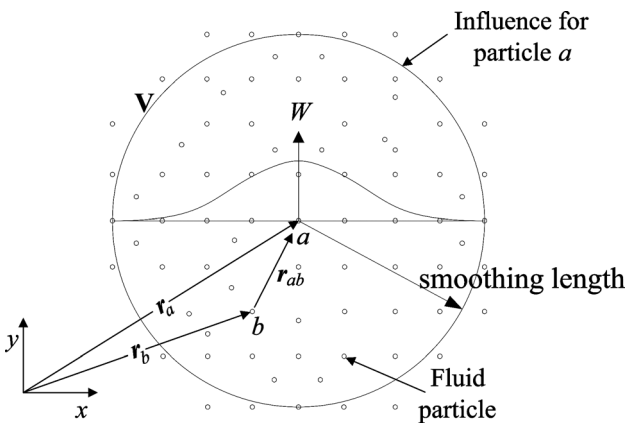

Fig. 1 Definition of SPH particle *a* in volume V

or weight function. The kernel approximation of a function $f(\boldsymbol{r})$ in SPH is defined as integral form over volume $\mathbf{V}$

$$f(\boldsymbol{r}) = \int_{\mathbf{V}} f(\boldsymbol{r}')\delta(\boldsymbol{r}-\boldsymbol{r}')d\boldsymbol{r}' \tag{19}$$

where f is a function of position vector $\boldsymbol{r}$ or $\boldsymbol{r}'$ over volume $\mathbf{V}$, and $\delta(\boldsymbol{r}-\boldsymbol{r}')$ is the Dirac delta function given by

$$\delta(\boldsymbol{r}-\boldsymbol{r}') = \begin{cases} 1 & \boldsymbol{r}=\boldsymbol{r}' \\ 0 & \boldsymbol{r}\neq\boldsymbol{r}' \end{cases} \tag{20}$$

If the Dirac delta function is replaced by the smoothing kernel W and a smoothing length h, approximated function $f_p(\boldsymbol{r})$ can be obtained

$$f_p(\boldsymbol{r}) = \int_{\mathbf{V}} f(\boldsymbol{r}')W(\boldsymbol{r}-\boldsymbol{r}',h)d\boldsymbol{r}' \tag{21}$$

where smoothing kernel W has to be satisfied with normalization condition as follows:

$$\int_{\mathbf{V}} W(\boldsymbol{r}-\boldsymbol{r}',h)d\boldsymbol{r}' = 1 \tag{22}$$

In Eq. (21), infinitesimal volume $d\boldsymbol{r}'$ can be defined follow relationship

$$m_a = \Delta\boldsymbol{r}_a\rho_a \tag{23}$$

where for location of particle a, m_a is a mass of the particle, $\Delta\boldsymbol{r}_a$ is a finite volume, and ρ_a is a density. When Eq. (23) is substituted into Eq. (21), approximated function $f_p(\boldsymbol{r})$ can be expressed summation form

$$f_p(\boldsymbol{r}) \cong \sum_b f(\boldsymbol{r}_b)W(\boldsymbol{r}-\boldsymbol{r}_b,h)\Delta\boldsymbol{r}_a \tag{24}$$

This equation can be represented over $|\boldsymbol{r}-\boldsymbol{r}'| < \kappa h$ field

$$f_p(\boldsymbol{r}) = \sum_b \frac{m_b}{\rho_b} f(\boldsymbol{r}_b)W(|\boldsymbol{r}-\boldsymbol{r}_b|,h) \tag{25}$$

where ρ_a is defined with smoothed kernel function

$$\rho_a = \sum_b m_b W_{ab} \tag{26}$$

and smoothing function of particle a evaluated by particle b

$$W_{ab} = W(\boldsymbol{r}_a-\boldsymbol{r}_b,h) \tag{27}$$

At particle a, the particle approximations for the gradient and divergence of Eq. (25) are

$$\nabla_a f_p(\boldsymbol{r}_a) = \sum_b \frac{m_b}{\rho_b} f(\boldsymbol{r}_b)\nabla_a W_{ab} \tag{28}$$

and

$$\nabla\cdot f_p(\boldsymbol{r}_a) = \sum_b \frac{m_b}{\rho_b} f(\boldsymbol{r}_b)\cdot\nabla_a W_{ab} \tag{29}$$

Well known momentum balance equation in the Navier–Stokes is defined as follows:

$$\frac{D\boldsymbol{v}(\boldsymbol{r}_a)}{Dt} = \frac{1}{\rho_a}\nabla_a\sigma(\boldsymbol{r}_a) \tag{30}$$

where $\boldsymbol{v}(\boldsymbol{r}_a)$ is velocity vector of particle a, and $\sigma(\boldsymbol{r}_a)$ is the total stress and it can be divided into isotropic pressure $p(\boldsymbol{r}_a)$ and viscous stress $\tau(\boldsymbol{r}_a)$

$$\sigma(\boldsymbol{r}_a) = -p(\boldsymbol{r}_a) + \tau(\boldsymbol{r}_a) \tag{31}$$

and viscous stress $\tau(\boldsymbol{r}_a)$ can be defined with viscosity $\mu(\boldsymbol{r}_a)$ and shear strain rate $\varepsilon(\boldsymbol{r}_a)$

$$\tau(\boldsymbol{r}_a) = \mu(\boldsymbol{r}_a)\varepsilon(\boldsymbol{r}_a) \tag{32}$$

Substitution Eq. (28) into Eq. (30), well known momentum balance equation in the Navier–Stokes equation are derived

$$\frac{D\boldsymbol{v}(\boldsymbol{r}_a)}{Dt} = \sum_b m_b\left(\frac{\sigma(\boldsymbol{r}_a)}{\rho_a^2} + \frac{\sigma(\boldsymbol{r}_b)}{\rho_b^2}\right)\nabla_a W_{ab} \tag{33}$$

Using Eqs. (30) and (31), Eq. (32) can be rewritten as follows:

$$\begin{aligned}\frac{D\boldsymbol{v}(\boldsymbol{r}_a)}{Dt} = &-\sum_b m_b\left(\frac{p(\boldsymbol{r}_a)}{\rho_a^2} + \frac{p(\boldsymbol{r}_b)}{\rho_b^2}\right)\nabla_a W_{ab} \\ &+ \sum_b m_b\left(\frac{\mu(\boldsymbol{r}_a)\varepsilon(\boldsymbol{r}_a)}{\rho_a^2} + \frac{\mu(\boldsymbol{r}_b)\varepsilon(\boldsymbol{r}_b)}{\rho_b^2}\right)\nabla_a W_{ab}\end{aligned} \tag{34}$$

In Eq. (34), first RHS is approximation of pressure and second RHS is expressed viscous force. For simplify viscosity, Morris [26] proposed an equation

$$\begin{aligned}\frac{D\boldsymbol{v}(\boldsymbol{r}_a)}{Dt} = &-\sum_b m_b\left(\frac{p(\boldsymbol{r}_a)}{\rho_a^2} + \frac{p(\boldsymbol{r}_b)}{\rho_b^2}\right)\nabla_a W_{ab} \\ &+ \sum_b m_b\left(\frac{\mu(\boldsymbol{r}_a)+\mu(\boldsymbol{r}_b)\boldsymbol{v}(\boldsymbol{r}_{ab})}{\rho_a\rho_b}\right)\left(\frac{1}{|\boldsymbol{r}_{ab}|}\frac{\partial W_{ab}}{\partial\boldsymbol{r}_{ab}}\right)\end{aligned} \tag{35}$$

where $\boldsymbol{r}_{ab} = \boldsymbol{r}_a - \boldsymbol{r}_b$ is the distance between the two particles

4.2 Smooth Kernel Function. On the other hand, the selection of smooth kernel function is very important factor in SPH method because it is related with numerical stability and accuracy. For this time, many smooth functions have been introduced. The most used smoothing kernel function is B-spline function proposed by Monaghan and Lattanzio [27].

$$W(\boldsymbol{r}-\boldsymbol{r}',h) = a_f\begin{cases} \frac{2}{3} - (\boldsymbol{r}-\boldsymbol{r}')^2 + \frac{1}{2}(\boldsymbol{r}-\boldsymbol{r}')^3 & 0 \le (\boldsymbol{r}-\boldsymbol{r}') < 1 \\ \frac{1}{6}(2-\boldsymbol{r})^3 & 1 \le (\boldsymbol{r}-\boldsymbol{r}') < 2 \\ 0 & (\boldsymbol{r}-\boldsymbol{r}') \ge 2 \end{cases} \tag{36}$$

where factor a_f is replaced by $(1/h)$ for one dimensional, $(15/7\pi h^2)$ for two dimensional, and $(3/2\pi h^3)$ for three-dimensional. However, this function has a shortcoming that the second derivative of the function is linear. This leads to a nonsmoothness problem at inflection point. For this reason, higher order smoothed function was proposed by Morris [26]

$$W(\boldsymbol{r}-\boldsymbol{r}',h) = a_f\begin{cases} (3-(\boldsymbol{r}-\boldsymbol{r}'))^5 - 6(2-(\boldsymbol{r}-\boldsymbol{r}'))^5 + 15(1-(\boldsymbol{r}-\boldsymbol{r}'))^5 & 0 \le (\boldsymbol{r}-\boldsymbol{r}') < 1 \\ (3-(\boldsymbol{r}-\boldsymbol{r}'))^5 - 6(2-(\boldsymbol{r}-\boldsymbol{r}'))^5 & 1 \le (\boldsymbol{r}-\boldsymbol{r}') < 2 \\ (3-(\boldsymbol{r}-\boldsymbol{r}'))^5 & 2 \le (\boldsymbol{r}-\boldsymbol{r}') < 3 \\ 0 & (\boldsymbol{r}-\boldsymbol{r}') > 3 \end{cases} \tag{37}$$

where factor a_f is $(120/h)$, $(7/478\pi h^2)$, $(3/359\pi h^3)$ for one, two, and three-dimensional, respectively.

5 Coupling Method

In order to solve behavior of saturated porous media, above introduced mixed FEM can be used with continuum properties; moreover DEM and SPH can be used for solving solid particle motion and fluid flow on discontinuum level, respectively. In concurrent multiscale method, these independent numerical methods are interacted on entire domain by coupling method. Therefore, it is necessary to define relationships between these numerical approaches. In this paper, we introduce meshed discrete element which is based on FEM, DEM, and SPH. The main idea is that SPH particles are superposed with a discrete element and its motions are governed by the Newton's second law. This approach has following advantages;

(1) Arbitrary shape element can be used to describe solids on discontinuum level: In the early DEM, the shape of particles are rigid disk or rigid spherical, and that should be clustered by constitutive relationship between particles; however this is not enough to represent real solid phase in porous media because it is difficult to define constitutive relationship by forces. On the contrary, the proposed discrete element is no limitation to apply complex shape since it can be express that via mesh generation.
(2) It is not necessary to develop detection and contact algorithms for approaching particles: The detection of general DEM spends much computational time in order to calculate contact forces; moreover, contact forces can be missed when large time increments are used because near particles are moved fast. In computational point of view, numerical inefficiency can be occurred from this problem. The proposed discrete element can overcome this limitation without contact detection algorithm because SPH particles placed in discrete element play a role to detect approaching elements in their smoothed length. According to this process, repulse forces are generated, and this can be converted contact forces in a discrete element.

5.1 Meshed Discrete Element. The concept of the governing equations is started from the equation of motion for DEM. Assuming that not only an individual particle i in DEM is composed with FE but also damping effect is not considered, Eq. (12) can be defined as follows:

$$m_i\ddot{\boldsymbol{u}}_i + k_i\boldsymbol{u}_i = \boldsymbol{F}_i \tag{38}$$

where k_i is stiffness for a particle i, $\boldsymbol{u}_i$ is displacement for the in particle.

In general, if discrete elements, which have arbitrary shape, are contact, singularity at corners can be occurred during solving contact force $\boldsymbol{F}_{ij}^c$ in Eq. (17) because surface normal vector is not defined on all surface points (Fig. 2). This problem is more severe in arbitrary three-dimensional elements which have more corners.

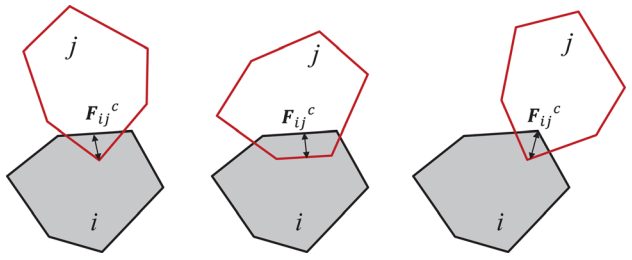

Fig. 2 A variety of contact (left) corner to line, (center) line to line, and (right) corner to corner

In order to overcome this problem, the concept of repulse force in SPH particles is used to a meshed discrete element. Namely, contact force is occurred by dense SPH particles in a meshed discrete element when other discrete elements including SPH particles are approaching.

In order to define contact force $\boldsymbol{F}_{ij}^c$ between discrete elements, the concept can be started from relationship between surface traction of solid boundary $\boldsymbol{t}$ and prescribed fluid pressure p (positive in compression) as follows:

$$\boldsymbol{t} = -p\boldsymbol{n}_s = p\boldsymbol{n} \tag{39}$$

where $\boldsymbol{n}_s$ is the outward normal vector to the solid phase and $\boldsymbol{n}$ is the outward normal vector to the fluid phase as Fig 3.

Since the proposed discrete element can be divided into meshed finite elements, the governing Eq. (38) including external force, contact force, and gravity force can be represented into weak form in finite element procedure with test functions for solid displacements $\delta\boldsymbol{u}^s$, which is derived by Dirichlet boundary conditions for displacements of discrete elements and Neumann boundary conditions for prescribed traction, as follows:

$$\int_\Omega \left[\rho_s\delta\boldsymbol{u}^s\cdot\ddot{\boldsymbol{u}}^s + \frac{\partial\delta\boldsymbol{u}^s}{\partial\boldsymbol{x}} : \boldsymbol{\sigma}\right]d\Omega = -\int_{\Gamma_t}\delta\boldsymbol{u}^s\cdot\boldsymbol{t}d\Gamma + \int_{\Gamma_t}\delta\boldsymbol{u}^s\cdot\boldsymbol{n}pd\Gamma + \int_\Omega\rho_s\delta\boldsymbol{u}^s\cdot\boldsymbol{b}d\Omega \tag{40}$$

where ρ_s is density of solid, $\ddot{\boldsymbol{u}}^s$ is acceleration vector, $\boldsymbol{\sigma}$ is stress tensor, $\boldsymbol{b}$ is body force vector, Ω is solid domain, and Γ_t is boundary on solid phase.

Then, using the Galerkin discretization method, Eq. (40) can be expressed into discrete formulation as follows:

$$\mathbf{M}\ddot{\boldsymbol{u}}^s + \mathbf{K}\boldsymbol{u}^s = -\boldsymbol{F}^e + \mathbf{Q}\boldsymbol{p}^f + \boldsymbol{F}^g \tag{41}$$

where

$$\mathbf{M} = \int_\Omega (N^s)^T\rho^s N^s d\Omega$$

$$\mathbf{K} = \int_\Omega \left[(\nabla N^s\mathbf{C}_\mathrm{T}(\nabla N^s))^T\right]d\Omega$$

$$\boldsymbol{F}^e = \int_{\Gamma_t} N^s\boldsymbol{t}d\Gamma$$

$$\mathbf{Q} = \int_{\Gamma_t}(N^s)^T\boldsymbol{n}N^f d\Gamma$$

$$\boldsymbol{F}^g = \int_\Omega N^s\rho\boldsymbol{b}d\Omega$$

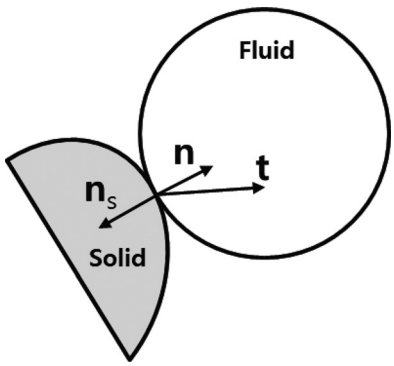

Fig. 3 Relationship between surface traction vectors

where the shape functions for fluid phase N^f is identical with N^s because fluid pressure at SPH particles is applied into each node in a finite element mesh. Moreover, contact force vector can be defined as $\boldsymbol{F}^c = \mathbf{Q}\boldsymbol{p}^f$. This plays a role a conversion fluid pressure of SPH particles to surface traction of discrete element.

For more detail description of the coupled matrix $\mathbf{Q}$, assuming that discrete element is generated by a 4-node isoparametric element, and 4 SPH particles are placed at each node as Fig 4.

Shape functions for the elements can be defined

$$N^s = N^f = [N_1 \quad N_2 \quad N_3 \quad N_4] \tag{42}$$

where

$$N_1 = \frac{1}{4}(1-\eta)(1-\xi)$$
$$N_2 = \frac{1}{4}(1+\eta)(1-\xi)$$
$$N_3 = \frac{1}{4}(1+\eta)(1+\xi)$$
$$N_4 = \frac{1}{4}(1-\eta)(1+\xi)$$

The contact force vector $\boldsymbol{F}^c$ can be represented on each boundary condition line

for B.C. line 0:

$$\boldsymbol{F}_0^c = \frac{h_d l_0}{2}\int_{-1}^{1}\begin{bmatrix}\frac{1-\eta}{2} & 0\\ 0 & \frac{1-\eta}{2}\\ \frac{1+\eta}{2} & 0\\ 0 & \frac{1+\eta}{2}\end{bmatrix}\begin{Bmatrix}n_{0x}\\ n_{0y}\end{Bmatrix}\begin{Bmatrix}\frac{1-\eta}{2} & \frac{1+\eta}{2}\end{Bmatrix}ds\begin{Bmatrix}p_0\\ p_1\end{Bmatrix} \tag{43}$$

where h_d is thickness of an element, l_0 is the length of between two adjacent node 0 and node 1, n_{0x} and n_{0y} is elements of normal vector on local boundary condition line 0

for B.C. line 1:

$$\boldsymbol{F}_1^c = \frac{h_d l_1}{2}\int_{-1}^{1}\begin{bmatrix}\frac{1-\xi}{2} & 0\\ 0 & \frac{1-\xi}{2}\\ \frac{1+\xi}{2} & 0\\ 0 & \frac{1+\xi}{2}\end{bmatrix}\begin{Bmatrix}n_{1x}\\ n_{1y}\end{Bmatrix}\begin{Bmatrix}\frac{1-\xi}{2} & \frac{1+\xi}{2}\end{Bmatrix}ds\begin{Bmatrix}p_1\\ p_2\end{Bmatrix} \tag{44}$$

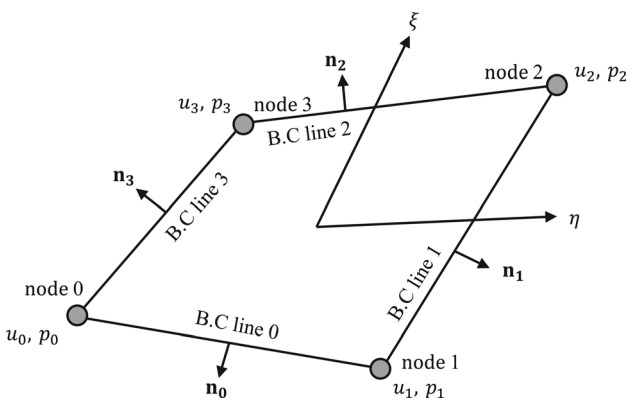

Fig. 4 Displacements and fluid pressures in natural coordinate $\eta - \xi$

for B.C. line 2:

$$\boldsymbol{F}_2^c = \frac{h_d l_2}{2}\int_{1}^{-1}\begin{bmatrix}\frac{1+\eta}{2} & 0\\ 0 & \frac{1+\eta}{2}\\ \frac{1-\eta}{2} & 0\\ 0 & \frac{1-\eta}{2}\end{bmatrix}\begin{Bmatrix}n_{2x}\\ n_{2y}\end{Bmatrix}\begin{Bmatrix}\frac{1+\eta}{2} & \frac{1-\eta}{2}\end{Bmatrix}ds\begin{Bmatrix}p_2\\ p_3\end{Bmatrix} \tag{45}$$

for B.C. line 3:

$$\boldsymbol{F}_3^c = \frac{h_d l_3}{2}\int_{1}^{-1}\begin{bmatrix}\frac{1+\xi}{2} & 0\\ 0 & \frac{1+\xi}{2}\\ \frac{1-\xi}{2} & 0\\ 0 & \frac{1-\xi}{2}\end{bmatrix}\begin{Bmatrix}n_{3x}\\ n_{3y}\end{Bmatrix}\begin{Bmatrix}\frac{1+\xi}{2} & \frac{1-\xi}{2}\end{Bmatrix}ds\begin{Bmatrix}p_3\\ p_0\end{Bmatrix} \tag{46}$$

These forces are applied into each node in an element, and this is deformed or moved by Eq. (41). The accurate forces can be obtained when dense SPH particles are placed into the discrete element.

On the other hand, fluid pressure vector $\boldsymbol{F}^f$ in Eq. (14) between fluid particle and DEM element can be ignored in this method because the interaction between fluid particle and imposed particles are already applied into contact forces. The concept of proposed discrete element is showed in Fig 5. Approaching discrete elements are detected by embedded SPH particles, and conversed contact forces by coupling matrix coupled matrix $\mathbf{Q}$ are responded to opposite discrete elements.

5.2 Time Integration. In order to perform dynamical analysis for proposed contact method, the explicit time integration by predictor-corrector time scheme (explicit method) is used. The predictor-corrector method is similar to the Newmark time integration which is implicit methods, and the most popular for dynamic analysis. However, this scheme has limited to choose small size time increment in order to numerical stability. The predictor-corrector method is used in proposed SPH and DEM method, respectively, as follows:

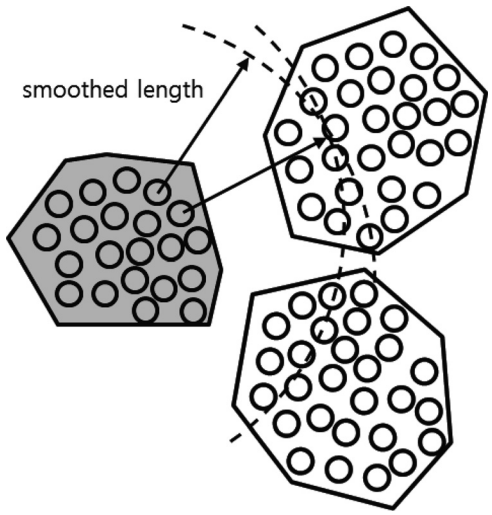

Fig. 5 Discrete element embedded SPH particles

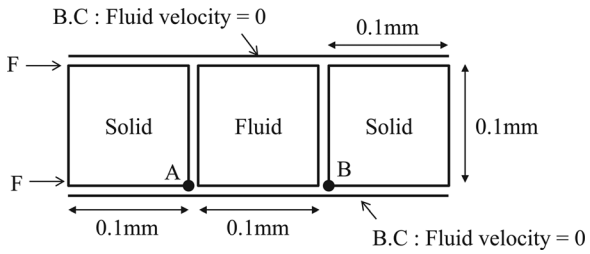

Fig. 6 Two discrete elements and SPH particles

Step 1: The acceleration and density in SPH, and lumped mass matrix, stiffness matrix, and force vector in DEM are calculated.

Step 2: In predictor step, predict velocity $\dot{\boldsymbol{u}}_{pre}$ is evaluated by calculated velocity $\dot{\boldsymbol{u}}_n$ and acceleration $\ddot{\boldsymbol{u}}_n$ in previous step n.

$$\dot{\boldsymbol{u}}_{pre} = \dot{\boldsymbol{u}}_n + \frac{\Delta t}{2}\ddot{\boldsymbol{u}}_n \tag{47}$$

where Δt is a time increment.

Step 3: Acceleration $(D\boldsymbol{v}(\boldsymbol{r}_a)/Dt)$ in Eq. (35) and $\ddot{\boldsymbol{u}}_{n+1}$ are evaluated. The predict velocity $\dot{\boldsymbol{u}}_{\text{pre}}$ is substituted into the velocity in viscosity term in Eq. (35). Moreover if damping effect is ignored in proposed analysis, the acceleration of proposed discrete element is straightforwardly obtained through lumped mass matrix in Eq. (41) as follows:

$$\ddot{\boldsymbol{u}}^s_{n+1} = \mathbf{M}^{-1}_{n+1}(-\boldsymbol{F}^e + \mathbf{Q}\boldsymbol{p}^f + \boldsymbol{F}^g - \mathbf{K}\boldsymbol{u}^s) \tag{48}$$

where mass matrix $\mathbf{M}$ has only lumped diagonal density.

Step 4: Velocity $\dot{\boldsymbol{u}}_{n+1}$ and displacements $\boldsymbol{u}_{n+1}$ for step $n+1$ are calculated by following equations:

$$\dot{\boldsymbol{u}}_{n+1} = \dot{\boldsymbol{u}}_{\text{pre}} + \frac{\Delta t}{2}\ddot{\boldsymbol{u}}_{n+1} \tag{49}$$

$$\boldsymbol{u}_{n+1} = \boldsymbol{u}_n + \Delta t\dot{\boldsymbol{u}}_n + \frac{\Delta t^2}{2}\ddot{\boldsymbol{u}}_{n+1} \tag{50}$$

Finally, positions of SPH particles and nodes of discrete element are updated by calculated displacement $\boldsymbol{u}_{n+1}$.

6 Numerical Examples

The verification of the proposed coupling method is performed by developed C++ codes, and the total of two models considering coupling relationship between meshed discrete elements and SPH particles are simulated. For this, in early introduced discrete element, which is embedded by SPH particles, is used.

6.1 Two Rigid Discrete Elements and SPH Particles. In this example, a coupled problem between two rigid discrete element for solid and SPH particles for fluid is simulated. Moving rigid discrete elements are interacted with SPH particles. Pressure for internal SPH particles in discrete element is applied into fluid particles of SPH, and fluid particles also transfer its pressures to another discrete element. In Fig. 6, fluid phase is closed by solid phases and boundary condition. The rigid discrete elements have one mesh, which has 4 nodes, and each discrete element has 81 internal SPH particles and 4 external SPH particles. Moreover, 83 SPH particles are placed in fluid phase. Space of internal SPH particles, external SPH particles, and fluid particles are 0.02 mm, 0.1 mm, and 0.02 mm, respectively. Moreover, the total of 62 boundary particles of which fluid velocity is zero are imposed top and bottom, and it has 0.02 mm interval. Material properties for solid are that the elastic modulus is 1×10^8 Pa, the Poisson ratio is 0.48, and the density is 2000 kg/m^3, moreover for fluid are that density of fluid is 1000 kg/m^3 and viscosity is 1×10^{-1}kg/m s. External forces 0.0001 N are prescribed on left side of left solid phase after SPH particles are a steady state condition. For explicit time integration, time increment Δt is used as 0.001 second for total time 60 seconds.

Figure 7 shows that the fluid pressure increment according to elapsed time at point A and point B in Fig 6. Two rigid solid discrete elements are first prescribed by fluid pressures of SPH particles during 20 seconds, and then the discrete elements are under a steady state condition as results of NF-point A in Fig 7. The reason of this phenomenon is that initial arranged SPH particles is

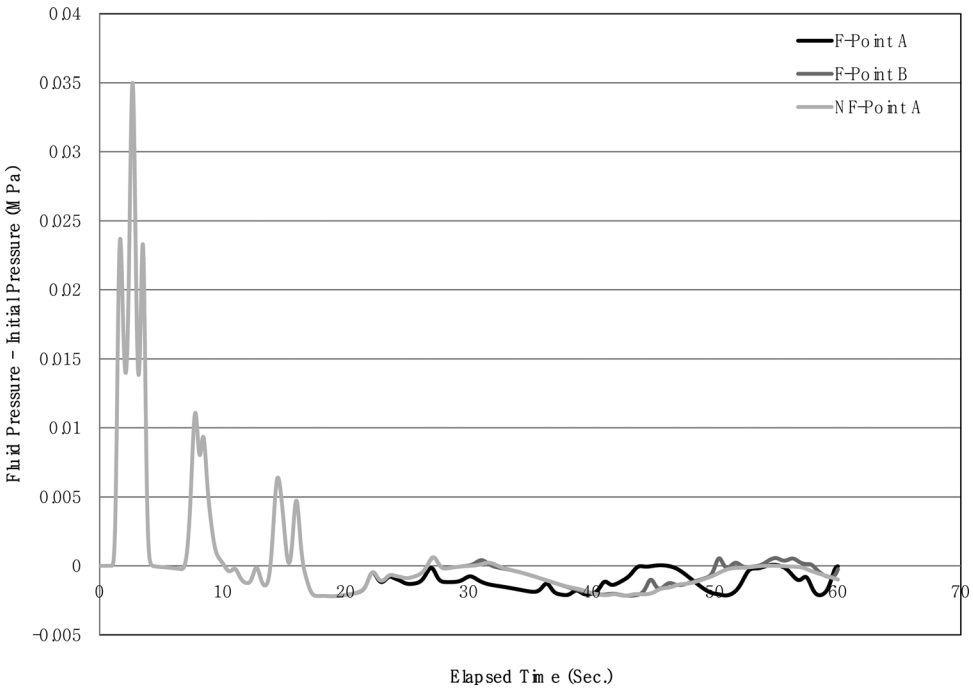

Fig. 7 Fluid pressure for elapsed time at point A and point B (the F-point A and the F-point B are results of model prescribed external force, and the NF-point A is result of model without prescribed external forces)

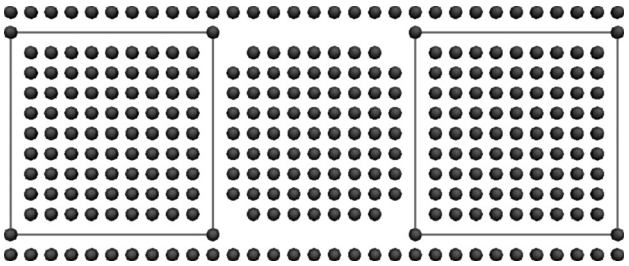

Fig. 8 0 second

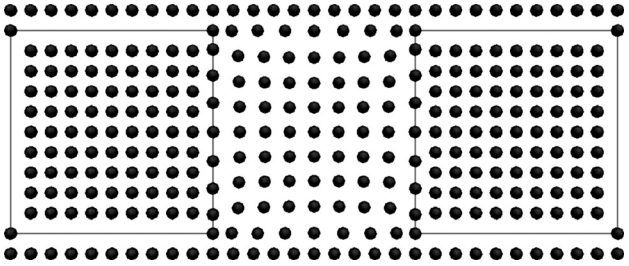

Fig. 9 1.5 seconds

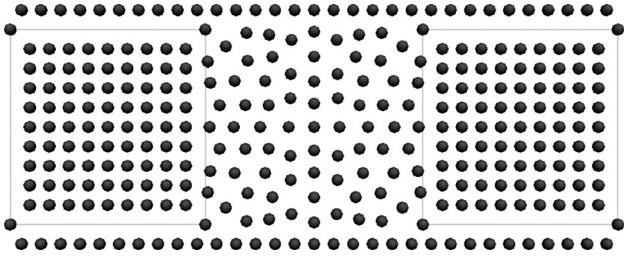

Fig. 10 20 seconds

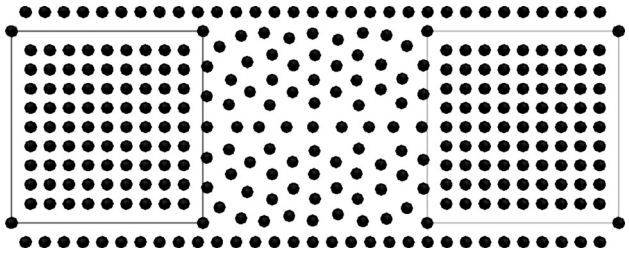

Fig. 11 30 seconds

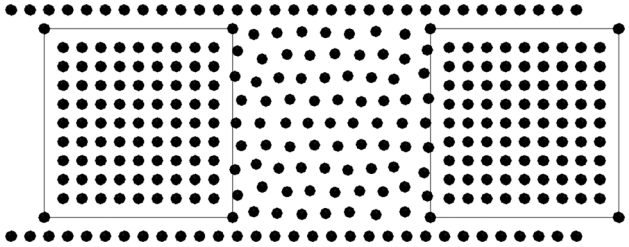

Fig. 12 60 seconds

spread by repulse forces, which is occurred from relationship between boundary SPH particles and fluid SPH particles, to reach the steady state condition as from Figs. 8–10. After a steady state condition, a left rigid discrete element in Fig 6 is moved by prescribed external forces. However, since there are no boundary conditions for moving discrete element, pressures at both point A and point B are nearly identical. This means that velocity of rigid discrete elements and SPH particles are almost the same. Figures 11 and 12 show that displacements of both discrete elements are almost identical, as well.

Figure 13 shows velocity at point A and point B. Until about 16 seconds, velocity at point A is nearly identical with velocity at point B. After that, the aspect of graph for two points is similar to the aspect of NF-point A, but the gap between two particles is larger. The reason of difference velocity between point A and point B is related with denseness of SPH particles. This problem can be resolved by increasing SPH particles and boundary condition in order to prevent penetration of SPH particles; however, much computational cost can be occur.

6.2 Coupling With Mixed FEM, Discrete Elements and SPH Particles. In this example, a saturated porous medium considered both continuum level and discontinuum level is simulated. For this, the simulation of interaction between early introduced mixed FEM, proposed discrete element and SPH particles is carried out. In Fig 14, zone 3 composed with proposed discrete element and SPH particles is closed by two porous media on zone 1 and zone 2 as well as boundary conditions.

In zone 1 and zone 2 for continuum level, porous media are assumed the nearly incompressible and impermeable conditions, and mixed FEM is used. In mixed FEM, because this assumption can bring numerical instability, such as element locking by incompatibility condition between finite elements, we use mixed FEM proposed by Park and Tak [28] and Tak and Park [29]. In this mode, total 808 nodes and 600 finite elements are used. Left side of zone 1 is permeable condition, but other sides are impermeable condition. For nearly incompressible condition, both bulk modulus K^s and K^f at compressible matrix in Eq. (11) are used 1×10^{14} Pa, and Biot's constant $\alpha = 1$. In addition, porosity n in Eq. (11) is used as 0.3. In addition, for nearly impermeable condition, permeability parameter which is diagonal entries of permeability tensor $\mathbf{k}$ at drainable matrix $\mathbf{D}$ in Eq. (11) is 1×10^{-17} m/s. Other properties are used that elastic modulus is 3×10^7 Pa, Poission ratio is 0.48, density of solid is 2000 kg/m^3, density of fluid is 1000 kg/m^3, and viscosity is 1×10^{-1}kg/ms.

In zone 3, solid motion and fluid flow are modeled by proposed discrete element and SPH particles, respectively. Material properties for solid are that the elastic modulus is 1×10^9 Pa, the Poisson ratio is 0.48, and the density is 2000 kg/m^3, moreover for fluid are that density of fluid is 1000 kg/m^3 and viscosity is 1×10^{-1} kg/m s. On this phase, there are 3 solid discrete elements which are arbitrary shapes, and it is divided by finite element mesh. In each mesh, 16 internal SPH particles are placed. In addition, total 167 SPH particles for fluid flow and 81 SPH particles for boundary condition are used. It is assumed that solid is rigid body and fluid is incompressible. Material properties of discrete element and SPH particles are same as that of previous introduced example. External force $\boldsymbol{F}^e = 1$Pa is applied into left side on zone 1, and it is prescribed at time 0. Time increment Δt is used as 0.0005 seconds.

Figure 15 shows that fluid pressure for elapsed time. In theoretical view point, for nearly incompressible and impermeable condition, fluid pressures that occur in a porous medium are identical to applied pressure. Namely, fluid pressure on a total domain should be 1 Pa of which magnitude is same as external force. The results at F-point A and F-point B are presented fluctuation, but the pattern is similar. Especially, before 10 seconds, the quantity of fluid pressure increment nearly agrees with results without external forces. However, the difference between fluid pressure with forces and it without forces becomes larger during time increment; also, fluid pressure is not converged to 1 Pa. This problem is related

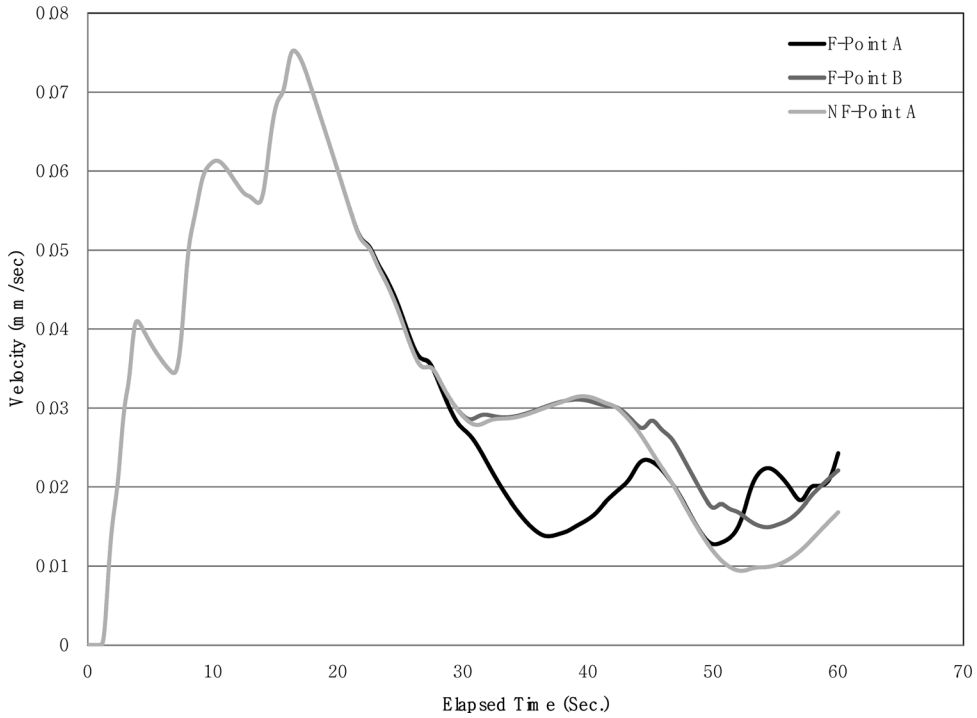

Fig. 13 Velocity for elapsed time at point A and point B

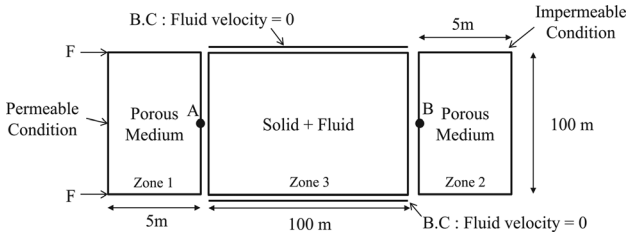

Fig. 14 Two discrete elements and SPH particles

with numerical instability of proposed method under the incompressible and impermeable condition. The discrete elements in zone 3 are interacted with SPH particles and that are moved and deformed in spite of high elastic modulus and Poisson ratio 0.48 as Figs. 16–19. In fact, rigid body motion on discontinumm level can be simulated by using higher elastic modulus and poisson ratio 0.5. However if stiffness of discrete elements is infinite, SPH particles are unstable condition because repulse force becomes also infinite. Consequently, appropriate material properties for solid should be carefully chosen to escape the instability.

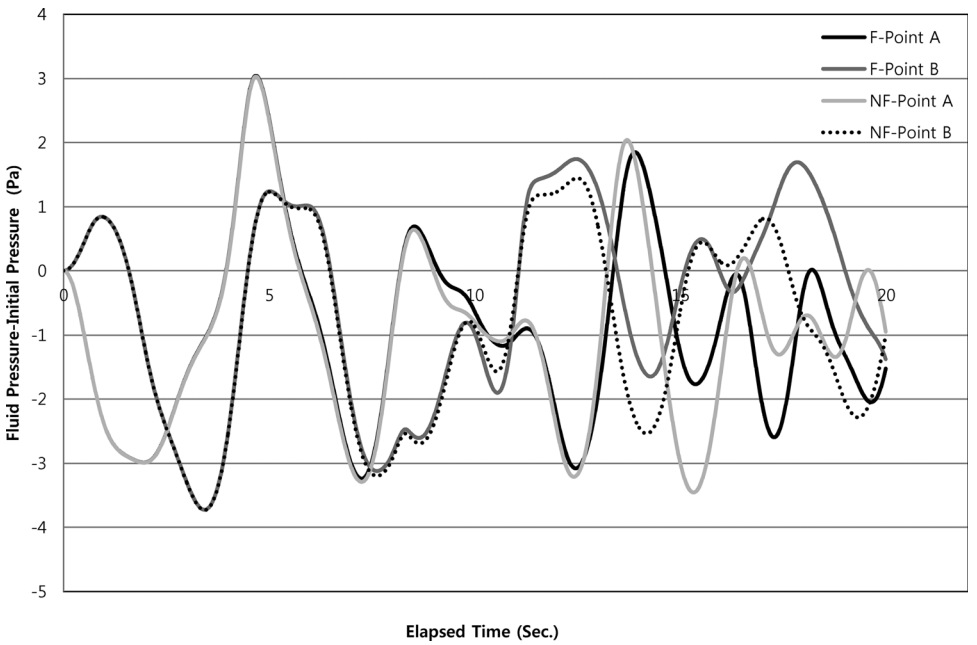

Fig. 15 Fluid pressure for elapsed time at point A and point B

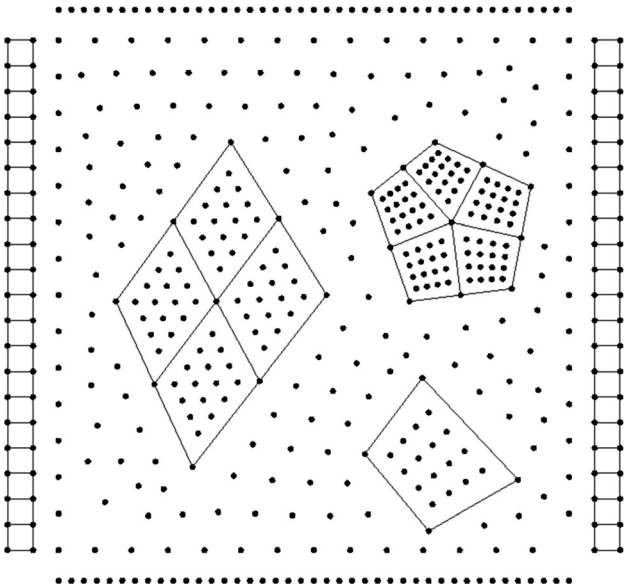

Fig. 16 0 seconds

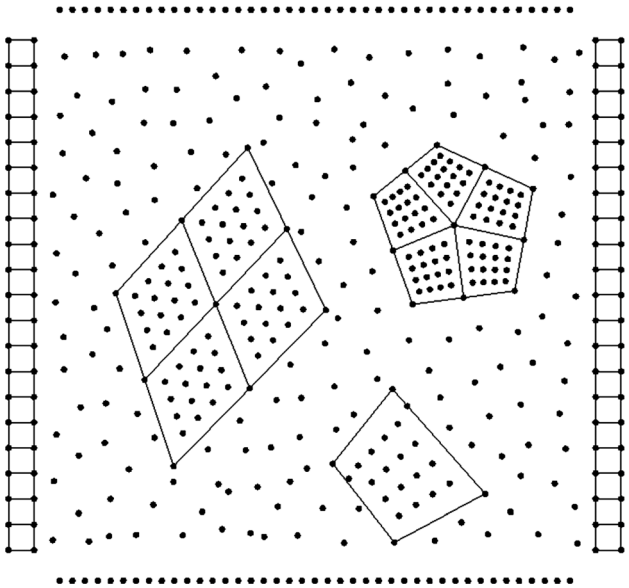

Fig. 18 10 seconds

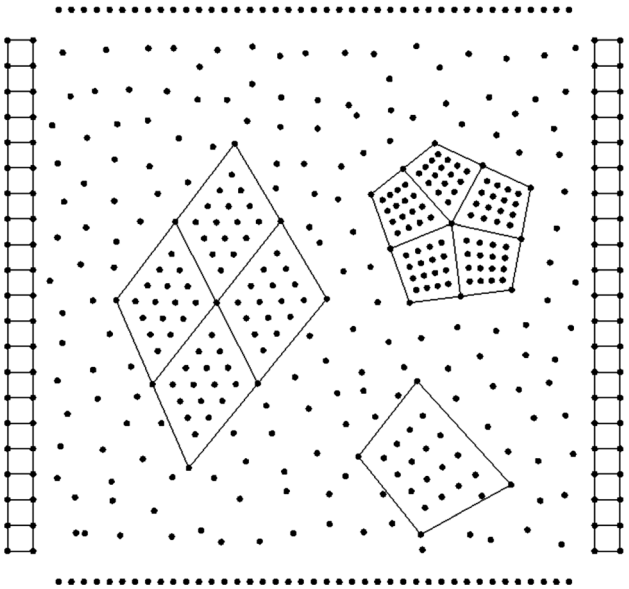

Fig. 17 5 seconds

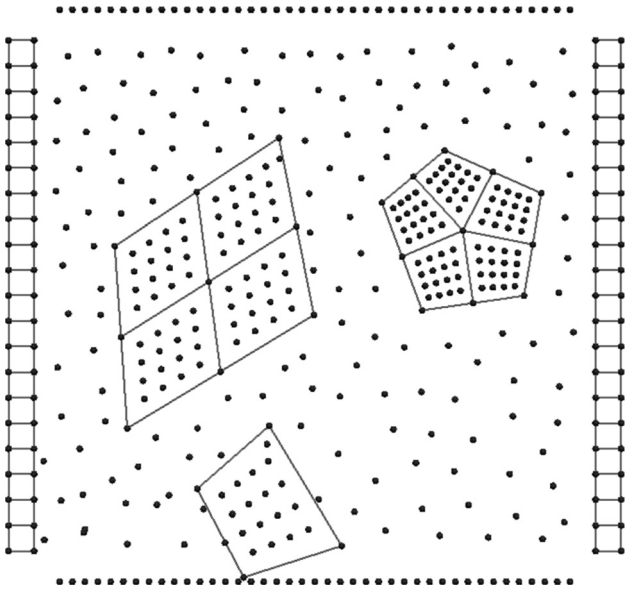

Fig. 19 20 seconds

7 Concluding Remarks

In this paper, coupling method to interact between FEM, DEM, and SPH was introduced. For this, we first reviewed mixed FEM, DEM as well as SPH method, and then we introduced coupling method based on discrete element. Moreover, in the simulation of porous media, this discrete element was showed good and reasonable results via simple models. Especially, proposed discrete element could be resolved contact problems with SPH particles on discontinuum level. However, numerical instability was occurred when mixed FEM on incompressible and impermeable condition is interacted. This is the reason why proposed discrete element cannot be supported to high compress on closed situation without free surface. Namely, the instability is related with deformation of solid phase. Therefore, it is necessary to develop a method to choose appropriate material properties in order to escape numerical instability.

The proposed method has many advantages that material crack, crumbing, concrete flow, and soil can be easily demonstrated if connect forces between proposed discrete elements are determined; however, previously a new parallel method suitable to the proposed method should be developed and verified through large size computational models.

Acknowledgment

This work was supported by the research fund of Hanyang University (HY-2012-I).

References

[1] Hou, T. Y., and Wu, X. H., 1997, "A Multiscale Finite Element Method for Elliptic Problems in Composite Materials and Porous Media," J. Comput. Phys., **134**(1), pp. 169–189.

[2] Schrefler, B. A., Gawin, D., and Pesavento, F., 2006, "A Multiphase Model for Concrete: Numerical Solutions and Industrial Applications," Progress in Industrial Mathematics at ECMI 2004, Mathematics in Industry, **8**, pp. 337–350.

[3] Kippe, V., Aarnes, J. E., and Lie, K. A., 2008, "A Comparison of Multiscale Methods for Elliptic Problems in Porous Media Flow," Comput. Geosci., **12**(3), pp. 377—398.

[4] Hajibeygi, H., and Jenny, P., 2009, "Multiscale Finite-Volume Method for Parabolic Problems Arising From Compressible Multiphase Flow in Porous Media," J. Comput. Phys., **228**(14), pp. 5129–5147.
[5] Zhang, P., Wu, Q. B., Pu, Y. B., Jiang, G. L., Zhan, J., and Wang, Y. M., 2010, "Water Transfer Characteristics During Methane Hydrate Formation and Dissociation Processes Inside Saturated Sand," J. Natural Gas Chem., **19**(1), pp. 71–76.
[6] El Shamy, U., and Zeghal, M., 2007, "A Micro-Mechanical Investigation of the Dynamic Response and Liquefaction of Saturated Granular Soils," Soil Dyn. Earthquake Eng., **27**(8), pp. 712–729.
[7] Zeghal, M., and El Shamy, U., 2008, "Liquefaction of Saturated Loose and Cemented Granular Soils," Powder Technol., **184**(2), pp. 254–265.
[8] Elmekati, A., and El Shamy, U., 2010, "A Practical Co-Simulation Approach for Multiscale Analysis of Geotechnical Systems," Comput. Geotech., **37**(4), pp. 494–503.
[9] Shafipour, R., and Soroush, A., 2008, "Fluid Coupled-DEM Modelling of Undrained Behavior of Granular Media," Comput. Geotech., **35**(5), pp. 673–685.
[10] Muguruma, Y., Tanaka, T., and Tsuji, Y., 2000, "Numerical Simulation of Particulate Flow With Liquid Bridge Between Particles (Simulation of Centrifugal Tumbling Granulator)," Powder Technol., **109**(1–3), pp. 49–57.
[11] Soulie, F., Cherblanc, F., El Youssoufi, M. S., and Saix, C., 2006, "Influence of Liquid Bridges on the Mechanical Behaviour of Polydisperse Granular Materials," Int. J. Numer. Anal. Meth. Geomech., **30**(3), pp. 213–228.
[12] Abu Bakar, N. F., Anzai, R., and Horio, M., 2009, "Direct Measurement of Particle Interaction Using Micro Particle Interaction Analyzer (MPIA)," Adv. Powder Technol., **20**(5), pp. 455–463.
[13] El Shamy, U., and Groger, T., 2008, "Micromechanical Aspects of the Shear Strength of Wet Granular Soils," Int. J. Numer. Anal. Meth. Geomech., **32**(14), pp. 1763–1790.
[14] Scholtes, L., Hicher, P. Y., Nicot, F., Chareyre, B., and Darve, F., 2009, "On the Capillary Stress Tensor in Wet Granular Materials," Int. J. Numer. Anal. Meth. Geomech., **33**(10), pp. 1289–1313.
[15] Tartakovsky, A., and Meakin, P., 2005, "Modeling of Surface Tension and Contact Angles With Smoothed Particle Hydrodynamics," Phys. Rev. E, **72**(2), pp. 1–9.
[16] Tartakovsky, A. M., and Meakin, P., 2006, "Pore Scale Modeling of Immiscible and Miscible Fluid Flows Using Smoothed Particle Hydrodynamics," Adv. Water Res., **29**(10), pp. 1464–1478.
[17] Tartakovsky, A. M., Meakin, P., Scheibe, T. D., and West, R. M. E., 2007, "Simulations of Reactive Transport and Precipitation With Smoothed Particle Hydrodynamics," J. Comput. Phys., **222**(2), pp. 654–672.
[18] Li, X., Chu, X., and Sheng, D. C., 2007, "A Saturated Discrete Particle Model and Characteristic-Based SPH Method in Granular Materials," Int. J. Numer. Meth. Eng., **72**(7), pp. 858–882.
[19] Berry, R. A., Martineau, R. C., and Wood, T. R., 2004, "Particle-Based Direct Numerical Simulation of Contaminant Transport and Deposition in Porous Flow," Vadose Zone J., **3**(1), pp. 164–169.
[20] Biot, M., 1941, "General Theory of Three Dimensional Consolidation," J. Appl. Phys., **12**, pp. 155–164.
[21] Terzaghi, K., 1925, *Erdbaumechanik auf Bodenphysikalischer Grundlage*, Leipzig u. Wien, F. Deuticke, Germany.
[22] Lewis, R., and Schrefler, B., 2000, *The Finite Element Method in the Static and Dynamic Deformation and Consolidation of Porous Media*, Wiley, New York.
[23] Cundall, P., and Strack, O., 1979, "A Discrete Numerical Model for Granular Assemblies," Geotechnique, **29**(1), pp. 47–65.
[24] Rojek, J., and Õnate, E., 2007, "Multiscale Analysis Using a Coupled Discrete/Finite Element Model," Interaction and Multiscale Mechanics, **1**, pp. 1–31.
[25] Hertz, H., 1826, "Über die Berührung fester elastischer Körper," Journal für die reine und angewandte Mathematik, **92**, pp. 156–171.
[26] Morris, J., 1966, *Analysis of Smoothed Particle Hydrodynamics With Applications*, PhD thesis, Monash University, Melbourne, Australia.
[27] Monaghan, J., and Lattanzio, J., 1985, "A Refined Particle Method for Astrophysical Problems," Astron. Astrophys., **149**, pp. 135–143.
[28] Park, T., and Tak, M., 2010, "A New Coupled Analysis for Nearly Incompressible and Impermeable Saturated Porous Media on Mixed Finite Element Method: I. Proposed Method," KSCE J. Civil Eng., **14**(1), pp. 7–16.
[29] Tak, M., and Park, T., 2010, "A New Coupled Analysis for Nearly Incompressible and Impermeable Saturated Porous Media on Mixed Finite Element Method: II. Verifications," KSCE J. Civil Eng., **14**(1), pp. 17–24.